Supplemental Material: Aging in the long-range Ising model

Henrik Christiansen,[1,*] Suman Majumder,[1,†] Malte Henkel,[2,3,4,‡] and Wolfhard Janke[1,§]

[1] *Institut für Theoretische Physik, Universität Leipzig, IPF 231101, 04081 Leipzig, Germany*
[2] *Laboratoire de Physique et Chimie Théoriques (CNRS UMR 7019), Université de Lorraine Nancy, 54506 Vandœuvre-lès-Nancy Cedex, France*
[3] *Centro de Física Teórica e Computacional, Universidade de Lisboa, 1749-016 Lisboa, Portugal*
[4] *Max-Planck Institute for the Physics of Complex Systems, Nöthnitzer Str. 38, 01187 Dresden, Germany*

(Dated: September 17, 2020)

METHODS

For the Monte Carlo (MC) simulation of the LRIM given by the Hamiltonian

$$\mathcal{H} = -\frac{1}{2}\sum_i \sum_{j\neq i} J(r_{ij}) s_i s_j, \text{ with } J(r_{ij}) = \frac{1}{r_{ij}^{d+\sigma}}, \quad \text{(S.1)}$$

we introduce the kinetics via single-spin flips. A randomly chosen spin is flipped according to the standard Metropolis update with probability $\min[1, \exp(-\Delta E/T)]$, with the Boltzmann constant k_B set to unity. Here, T is the temperature and ΔE is the change in energy before and after the flip. $N = L^d$ (where L is the linear size of a hyper-cubic lattice) such attempts constitute one MC sweep, setting the time scale. Obviously, for the LRIM the calculation of the energy change is the rate limiting step, as it involves all the spins in the considered lattice. However, following our recent approach of storing the effective field for each spin and updating it only when a spin flip is accepted makes such simulation significantly faster [1]. Furthermore, to allow for simulations of system size up to $L = 4096$ in $d = 2$ dimensions, this update was parallelized using the shared-memory API OpenMP framework. Since systems with long-range interaction suffer severely from finite-size effects we additionally use Ewald summation [2–5] to implement periodic boundary conditions and thereby to increase the effective system size. An effective $J_{ij} \equiv J(r_{ij})$ is calculated once at the beginning of the simulation.

As an initial configuration at high temperature, we chose a square lattice with randomly distributed equal proportion of up and down spins. We chose $T = 0.1T_c$ as the quench temperature, where we extract T_c from the data presented in Ref. [3]. Using the scaling relation $C(r,t) \equiv \tilde{C}[r/\ell(t)]$ for the equal-time two-point correlation function $C(r,t) = \langle s_i s_j\rangle - \langle s_i\rangle\langle s_j\rangle$ one can estimate the characteristic length scale $\ell(t)$ from the decay of $C(r,t)$ as intersection with a constant value where here we choose $C[r = \ell(t), t] = 0.5$. All considered quantities such as $\ell(t)$ and $C(t,t_w)$ are averages over independent time evolutions, indicated, e.g., in Eq. (3) of the main article by $\langle\ldots\rangle$. The presented results are averaged over 50 independent runs for $L \leq 2048$ and 30 for $L = 4096$ (using different random number seeds).

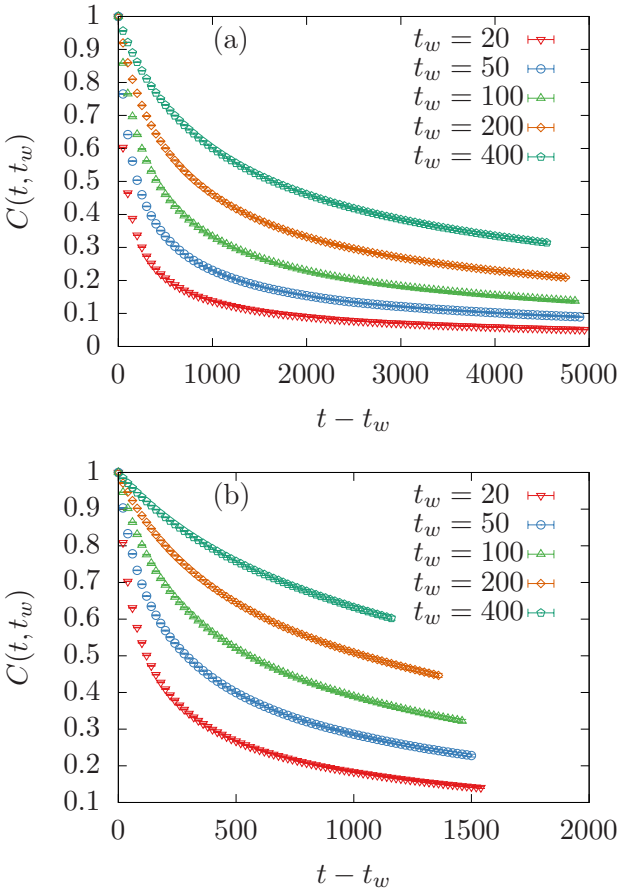

FIG. S1. Two-time correlator $C(t,t_w)$ plotted against $t - t_w$, illustrating the loss of time-translational invariance for (a) $\sigma = 1.5$ and $L = 2048$ and (b) $\sigma = 0.6$ and $L = 4096$.

ILLUSTRATION OF THE LOSS OF TIME-TRANSLATIONAL INVARIANCE

Figure S1 shows the two-time correlator $C(t,t_w)$ versus $t - t_w$, explicitly demonstrating the loss of time-translational invariance during coarsening. The data for larger t_w decay slower, i.e., the older the system is at the waiting time t_w, the longer in terms of t it needs to decorrelate.

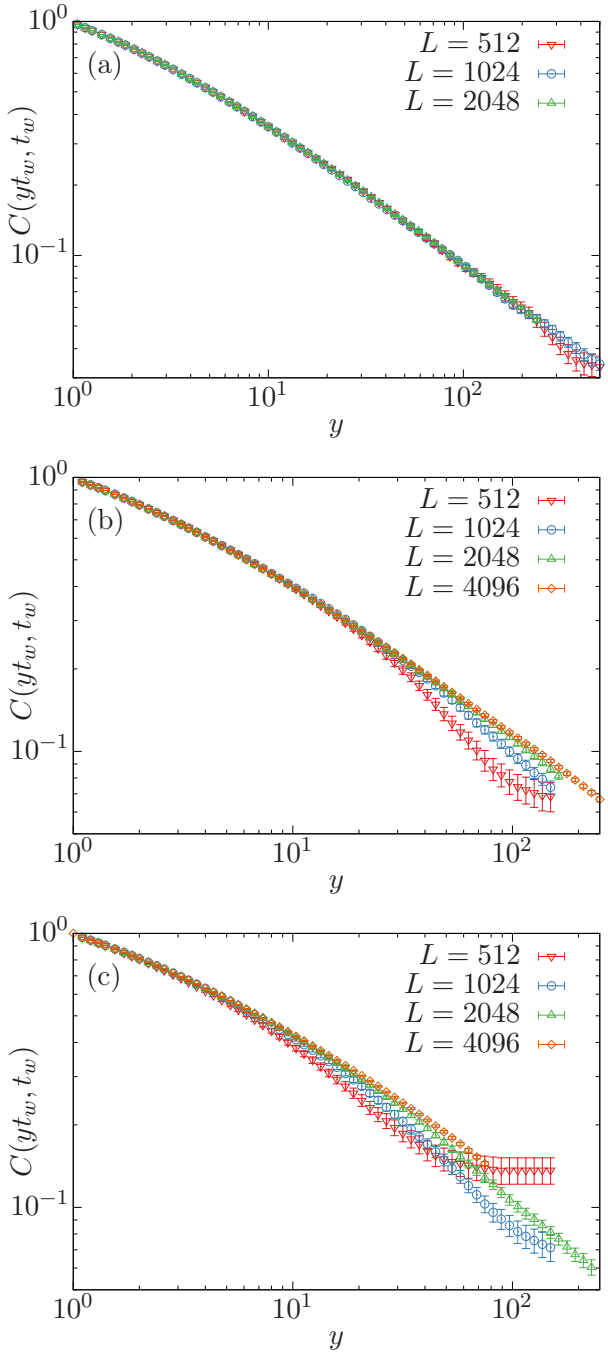

FIG. S2. As an illustration of finite-size effects, we show $C(yt_w, t_w)$ for fixed $t_w = 20$ by varying the system size L for (a) $\sigma = 1.5$, (b) $\sigma = 0.8$, and (c) $\sigma = 0.6$.

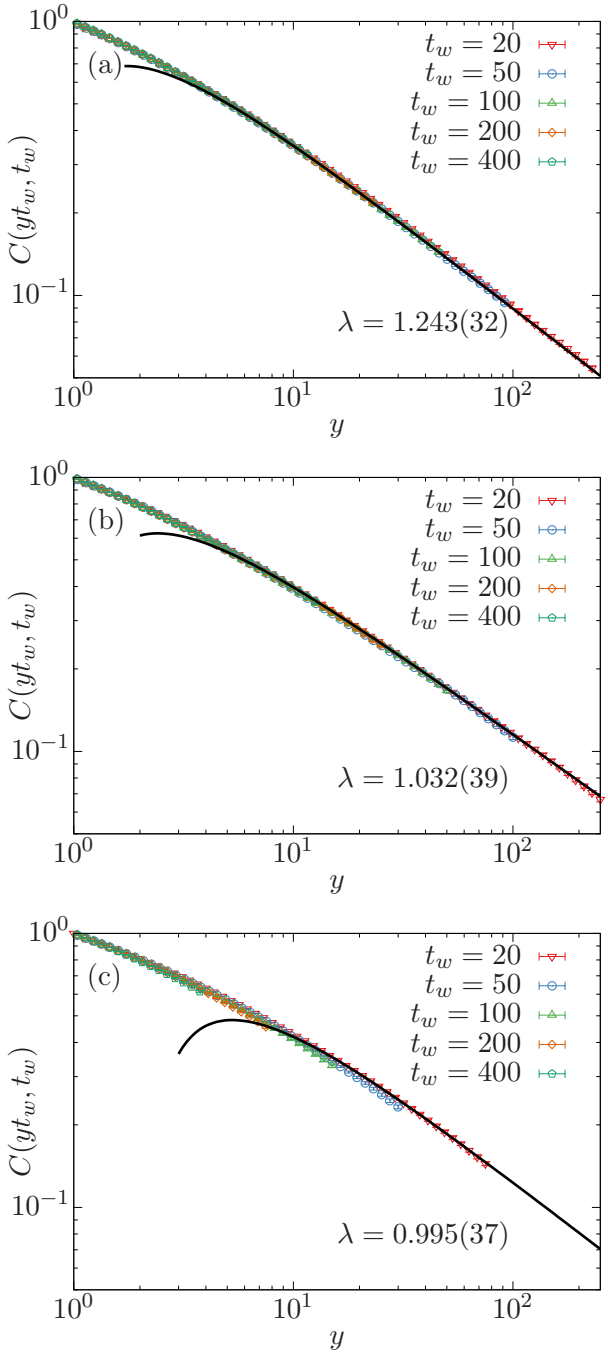

FIG. S3. Replot of Fig. 2 from the main article showing $C(yt_w, t_w)$ versus y for (a) $\sigma = 1.5$, (b) $\sigma = 0.8$, and (c) $\sigma = 0.6$. The adjustment we have made compared to Fig. 2 is that we plot the fit to ansatz (5) over a wider y-range. This illustrates to which extent a first-order correction can adjust for the bending of the data for small y and the deviation due to finite-size effect for large y.

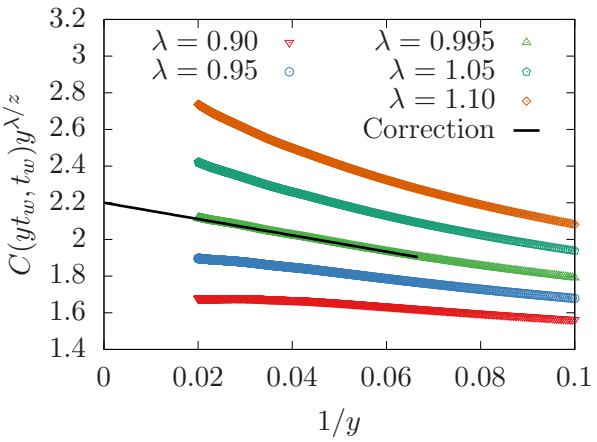

FIG. S4. Replot of Fig. 3(b) of the main article using narrower λ-values and a smaller $1/y$ range emphasizing the large y behavior. Shown is $C(yt_w, t_w)y^{\lambda/z}$ versus $1/y$ for $\sigma = 0.6$ and $L = 4096$.

FINITE-SIZE EFFECTS OF THE AUTOCORRELATION FUNCTION

In Fig. S2 we show $C(yt_w, t_w)$ versus y for (a) $\sigma = 1.5$, (b) $\sigma = 0.8$, and (c) $\sigma = 0.6$ with fixed $t_w = 20$ and varying L. For $\sigma = 1.5$ the data show the bulk behavior over a large y range, and only for $L = 512$ the data deviate by bending down at $y \approx 200$. The available data for $L = 1024$ and $L = 2048$ do not deviate, i.e., there are no detectable finite-size effects. For $\sigma = 0.8$ and $\sigma = 0.6$, the data for both $L = 512$ and $L = 1024$ undershoot from the bulk curve. This happens at larger y, the larger L. For $L = 2048$ this effect is hence less pronounced and for $L = 4096$ it can only be anticipated from these plots. Finally, because eventually the system reaches a configuration with spontaneous magnetization $m_{\rm eq}(T)$, the overlap and thereby autocorrelation function approaches a constant. Note that the data for smaller systems even cross the data of the bigger systems. This effectively limits the extent to which the data can undershoot from the bulk behavior for smaller y.

SIMPLE-AGING PLOTS WITH A LONGER RANGE OF THE FITTED FORM

In Fig. S3 we plot the fits to ansatz (5) shown in Fig. 2 of the main article over a wider y-range to demonstrate visually up to which extent the data may be described by this functional form. Shown is $C(yt_w, t_w)$ versus y for (a) $\sigma = 1.5$, (b) $\sigma = 0.8$, and (c) $\sigma = 0.6$. We see that towards small y the first-order correction can only describe the data down to a certain point $y_{\rm min}$ as discussed in the main article. Asymptotically this correction vanishes and the functional form approaches a pure power law. For large $y > y_{\rm max}$, the data deviate from the fit due to finite-size effects (cf. Fig. S2).

SMALLER $1/y$ RANGE FOR FIG. 3(b)

In Fig. S4 we replot Fig. 3(b) of the main article using a smaller $1/y$ range and two new λ values that are closer to the fitted value of $\lambda = 0.995(37)$. These two values $\lambda = 0.95$ and $\lambda = 1.05$ are chosen so that they roughly correspond to the error margins of the fitted λ. To be able to more easily compare with the plot in the main article, we have also again included $\lambda = 0.9$ and $\lambda = 1.1$. One clearly sees that the curves for $\lambda = 0.95$ show a downward bending, whereas the data for $\lambda = 1.05$ show signature of increasing slope. The data for $\lambda = 0.995$ is linear over a relatively long stretch of $1/y$ and well described by the fitted correction. This visually reconfirms $\lambda \approx 0.995$ and establishes the bounds $0.95 \leq \lambda \leq 1.05$.

ALTERNATIVE FORM OF SUB-AGING

Instead of using the analytically derived form of sub-aging with $h(t)$ as defined in the main article, one may use the more phenomenological form of t/t_w^μ (or $\ell(t)/\ell(t_w)^\mu$) to modify the scaling variable. In Fig. S5 we present $C(t, t_w)$ vs. t/t_w^μ for $\sigma = 0.6$ and $L = 4096$ with $\mu = 0.970, 0.976, 0.982$, and 0.99. Compared to using $h(t)$ the data collapse is worse and one effectively only shifts the crossing point of data for different t_w. This approach does thus not lead to better collapse.

TWO-TIME AUTOCORRELATORS FROM LOCAL SCALE-INVARIANCE WITH $z = 2$

According to local scale-invariance [6–9] the generic dynamical scaling which arises especially in aging systems far from equilibrium can be extended to a larger group of dynamical symmetries. For the phase-ordering kinetics of systems with short-ranged interactions, it is known that the dynamical exponent $z = 2$ [10, 11]. Then the Schrödinger group, which arises as dynamical symmetry of the free diffusion equation, is an example of an extended dynamical symmetry [6]. Numerous systems which physically realize Schrödinger invariance have been found, most notably phase-ordering kinetics in short-ranged Ising models in $d = 1, 2, 3$ dimensions, see [8, 9] and references therein. Here we discuss how the requirement of Schrödinger invariance restricts the two-time autocorrelator in phase-ordering kinetics.

Physically, it is the two-time or multi-time response functions which transform co-variantly under local scale-transformations. Turning to the two-time autocorrelator $C(t, t_w)$, after a quench to $T < T_c$ from a fully disordered

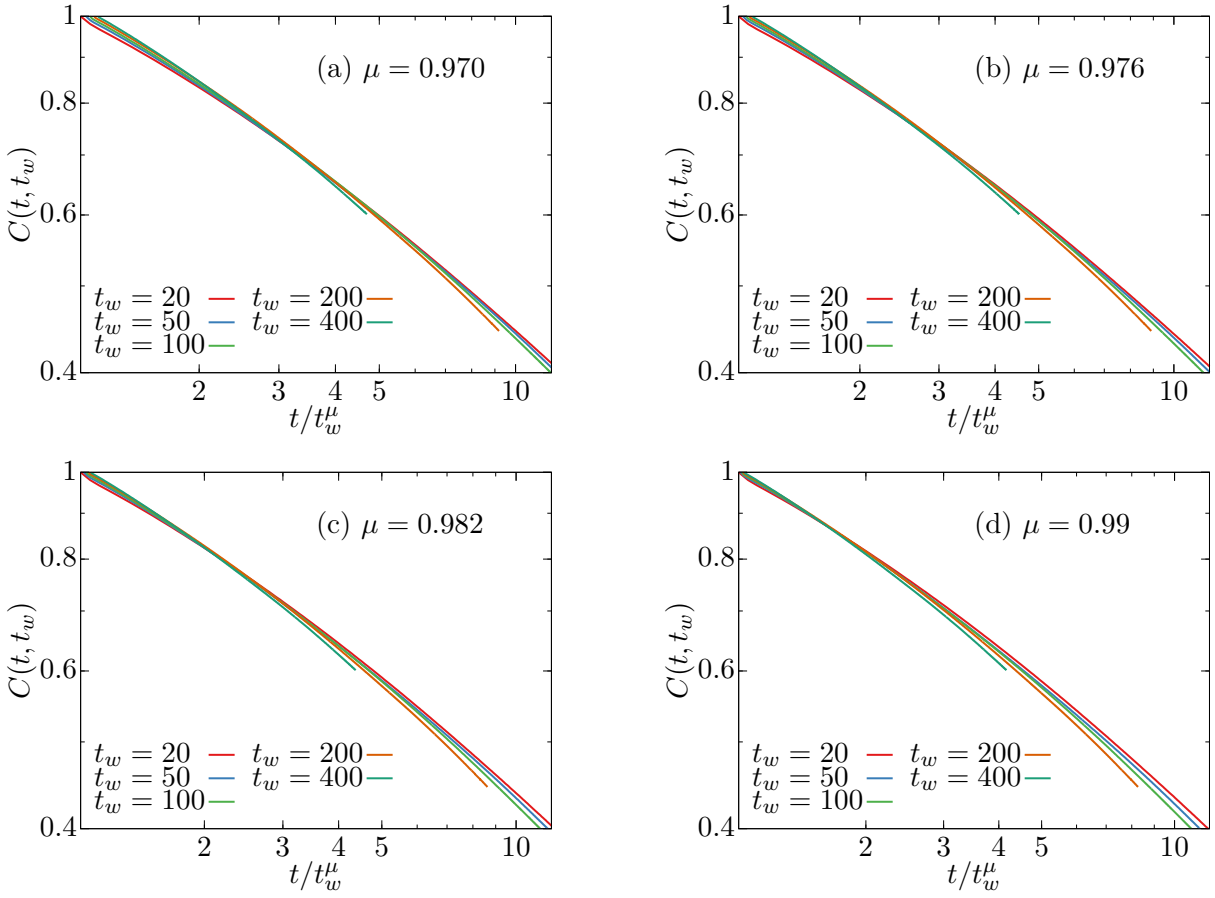

FIG. S5. Plots of $C(t, t_w)$ against t/t_w^μ for different values of μ mentioned in the figure. The data presented is for $\sigma = 0.6$ and $L = 4096$.

initial state, it can be expressed as [7]

$$C(t, t_w) = \frac{a_0}{2} \int_{\mathbb{R}^d} \mathrm{d}\vec{R}\, \mathcal{R}^{(3)}(t, t_w, t_{\mathrm{micro}}; \vec{R}) \tag{S.2}$$

where $\mathcal{R}^{(3)}$ is a three-point response function which in the context of Janssen-de Dominicis theory could be expressed as an average $\left\langle \psi(t, \vec{0})\psi(t_w, \vec{0})\widetilde{\psi}(t_{\mathrm{micro}}; \vec{R})^2 \right\rangle$ involving the order parameter ψ and the conjugate response operator $\widetilde{\psi}$. The form of that three-point response in turn is fixed up to a scaling function [6]. Furthermore, t_{micro} is a microscopic time scale and the amplitude a_0 measures the width of the initial correlator. Since for phase-ordering kinetics the temperature T is an irrelevant variable [11], the thermal heat bath merely furnishes corrections to scaling. In the dynamical scaling regime, the autocorrelator of phase-ordering kinetics can then be written as follows [7],

$$C(yt_w, t_w) = f_C(y) \;=\; y^{\lambda/2}(y-1)^{-\lambda} \mathbf{\Psi}\left(\frac{y+1}{y-1}\right), \tag{S.3}$$

$$\mathbf{\Psi}(w) = \int_{\mathbb{R}^d} \mathrm{d}\vec{R}\, \exp\left(-\frac{\mathcal{M}w}{2}\vec{R}^2\right) \Psi\left(\frac{\mathcal{M}}{2}\vec{R}^2\right) \tag{S.4}$$

where the undetermined scaling function $\Psi(\varrho)$ comes from the three-point response function mentioned above. Because of the known asymptotics $f_C(y) \sim y^{-\lambda/2}$ for $y \to \infty$, it follows that $\mathbf{\Psi}(1)$ exists and is finite. Denoting by S_d the surface of the hypersphere in d dimensions, Eq. (S.4) is re-written in spherical coordinates as

$$\mathbf{\Psi}(w) = \frac{S_d}{2}\left(\frac{2}{\mathcal{M}}\right)^{d/2} \int_0^\infty \mathrm{d}\varrho\;\; e^{-w\varrho}\, \varrho^{(d-2)/2} \Psi\left(\varrho\right) \tag{S.5}$$

and we also made explicit the non-universal metric factor $\mathcal{M}$. We recognize from this that $\mathbf{\Psi}$ is the Laplace transform of the function $\varrho^{(d-2)/2}\Psi(\varrho)$. Since it is well-known that a Laplace transform is infinitely often differentiable wherever it is defined, we can asymptotically expand in y [or equivalently around $w = 1$, see (S.3)] and find (the prime denotes the derivative)

$$\begin{aligned} f_C(y) &= \mathbf{\Psi}(1)\, y^{-\lambda/2}\left[1 + \left(\lambda + 2\frac{\mathbf{\Psi}'(1)}{\mathbf{\Psi}(1)}\right)\frac{1}{y} + \ldots\right] \\ &= f_{C,\infty}\, y^{-\lambda/2}\left(1 - \frac{A}{y} + \ldots\right) \end{aligned} \tag{S.6}$$

where we identified the constant A. This is the form (5) used in the text.

In order to estimate the amplitude A, we require some more input on the scaling function $\Psi(\varrho)$ in (S.4). First, we assume that for $\varrho \to \infty$, $\Psi(\varrho)$ grows more slowly than exponentially which is consistent with $\mathbf{\Psi}(1)$ being finite. Second, we recall that for $\varrho \to 0$ consistency with the asymptotic scaling of $f_C(y)$ requires that $\Psi(\varrho) \sim \varrho^{\lambda-d/2}$ [7]. Because of the known bound $\lambda \geq d/2$ [12, 13], $\Psi(\varrho)$ increases when $\varrho \ll 1$. We strengthen this to the requirement $\Psi'(\varrho) \geq 0$ also when ϱ is finite. Next, the integral representation (S.5) will become useful, via the following estimate

$$\begin{aligned}
&\int_0^\infty \mathrm{d}\varrho\ \ e^{-w\varrho}\,\varrho^{d/2}\Psi(\varrho) = -\frac{1}{w}\int_0^\infty \mathrm{d}\varrho\,\frac{\mathrm{d}}{\mathrm{d}\varrho}\left(e^{-w\varrho}\right)\varrho^{d/2}\Psi(\varrho)\\
&= -\underbrace{\left[\frac{e^{-w\varrho}}{w}\,\varrho^{d/2}\Psi(\varrho)\Big|_0^\infty\right]}_{=0} + \int_0^\infty \mathrm{d}\varrho\,\frac{e^{-w\varrho}}{w}\frac{\mathrm{d}}{\mathrm{d}\varrho}\left[\varrho^{d/2}\Psi(\varrho)\right]\\
&= \frac{1}{w}\int_0^\infty \mathrm{d}\varrho\, e^{-w\varrho}\left[\frac{d}{2}\varrho^{(d-2)/2}\Psi(\varrho) + \varrho^{d/2}\underbrace{\Psi'(\varrho)}_{\geq 0}\right]\\
&\geq \frac{1}{w}\frac{d}{2}\int_0^\infty \mathrm{d}\varrho\, e^{-w\varrho}\varrho^{(d-2)/2}\Psi(\varrho) \qquad \text{(S.7)}
\end{aligned}$$

where the two assumptions made on $\Psi(\varrho)$ were used explicitly and also for the estimation of the boundary terms after partial integration. With (S.5) we have

$$\frac{\mathbf{\Psi}'(w)}{\mathbf{\Psi}(w)} = -\frac{\int_0^\infty \mathrm{d}\varrho\, e^{-w\varrho}\varrho^{d/2}\Psi(\varrho)}{\int_0^\infty \mathrm{d}\varrho\, e^{-w\varrho}\varrho^{d/2-1}\Psi(\varrho)} \leq -\frac{1}{w}\frac{d}{2}. \qquad \text{(S.8)}$$

Setting $w = 1$, we then have the bound $\mathbf{\Psi}'(1)/\mathbf{\Psi}(1) \leq -d/2$. For the scaling function $f_C(y)$ of (S.6), this gives

$$f_C(y) \leq \mathbf{\Psi}(1) y^{-\lambda_C/2}\left[1 - \left(2\frac{d}{2} - \lambda\right)\frac{1}{y} + \ldots\right]. \qquad \text{(S.9)}$$

This upper bound on $f_C(y)$ gives a lower bound on the amplitude in (S.6)

$$A \geq d - \lambda. \qquad \text{(S.10)}$$

Indeed, it was argued long ago by Fisher and Huse [12] that $\lambda \leq d$. In models which respect this bound, (S.10) implies that $A \geq 0$. The validity of this Fisher-Huse bound was discussed in detail for phase-ordering systems [14]. However, for phase-separating model-B dynamics, this Fisher-Huse bound does not hold [13, 15].

Equation (S.6), along with (S.10), is reproduced in several exactly solvable models of phase-ordering with nearest-neighbour interactions and $z = 2$, see [8] for details.

For the 1D Glauber-Ising model at $T = 0$, we have

$$\begin{aligned}
f_C(y) &= \frac{2}{\pi}\arctan\sqrt{\frac{2}{y-1}}\\
&\simeq \frac{\sqrt{8}}{\pi}y^{-1/2}\left(1 - \frac{1}{6}\frac{1}{y} + \mathrm{O}(y^{-2})\right). \qquad \text{(S.11)}
\end{aligned}$$

Since $\lambda = 1$, the bound (S.10) $A \geq 0$ is consistent with the exact result $A = 1/6$.

For the spherical model in $d > 2$ dimensions and quenched to $T < T_c$, we have

$$\begin{aligned}
f_C(y) &= m_{\mathrm{eq}}^2\left[2y^{1/2}/(y+1)\right]^{d/2}\\
&\simeq m_{\mathrm{eq}}^2 2^{d/2} y^{-d/4}\left(1 - \frac{d}{2}\frac{1}{y} + \mathrm{O}(y^{-2})\right) \qquad \text{(S.12)}
\end{aligned}$$

with the equilibrium magnetization $m_{\mathrm{eq}}^2 = 1 - T/T_c$. Since $\lambda = d/2$, the bound (S.10) $A \geq d/2$ coincides with the exact result $A = d/2$.

Equation (S.6) can also be used as an ansatz for the spherical model with long-ranged interactions. There is a phase transition in the long-range universality class at a non-vanishing T_c provided $0 < \sigma < \min(d, 2)$ and $z = \sigma$. The scaling function of the two-time autocorrelator is

$$\begin{aligned}
f_C(y) &= m_{\mathrm{eq}}^2\left[2y^{1/2}/(y+1)\right]^{d/\sigma}\\
&\simeq m_{\mathrm{eq}}^2 2^{d/\sigma} y^{-d/(2\sigma)}\left(1 - \frac{d}{\sigma}\frac{1}{y} + \mathrm{O}(y^{-2})\right). \qquad \text{(S.13)}
\end{aligned}$$

Hence, $\lambda = d/2$ is σ-independent and we note that once more $A > 0$.

* henrik.christiansen@itp.uni-leipzig.de
† suman.majumder@itp.uni-leipzig.de
‡ malte.henkel@univ-lorraine.fr
§ wolfhard.janke@itp.uni-leipzig.de

[1] H. Christiansen, S. Majumder, and W. Janke, Phase ordering kinetics of the long-range Ising model, Phys. Rev. E **99**, 011301(R) (2019).

[2] P. Ewald, Die Berechnung optischer und elektrostatischer Gitterpotentiale, Ann. Phys. (Berl.) **369**, 253 (1921).

[3] T. Horita, H. Suwa, and S. Todo, Upper and lower critical decay exponents of Ising ferromagnets with long-range interaction, Phys. Rev. E **95**, 012143 (2017).

[4] E. Flores-Sola, M. Weigel, R. Kenna, and B. Berche, Cluster Monte Carlo and dynamical scaling for long-range interactions, Eur. Phys. J. Spec. Top. **226**, 581 (2017).

[5] W. Janke, H. Christiansen, and S. Majumder, Coarsening in the long-range Ising model: Metropolis versus Glauber criterion, J. Phys. Conf. Ser. **1163**, 012002 (2019).

[6] M. Henkel, Schrödinger invariance and strongly anisotropic critical systems, J. Stat. Phys. **75**, 1023 (1994).

[7] A. Picone and M. Henkel, Local scale-invariance and ageing in noisy systems, Nucl. Phys. B **688**, 217 (2004).

[8] M. Henkel and M. Pleimling, *Non-Equilibrium Phase Transitions, Vol. 2: Ageing and Dynamical Scaling far from Equilibrium* (Springer, Heidelberg, 2010), 2nd edition expected to be published in 2021.

[9] M. Henkel, From dynamical scaling to local scale-invariance: A tutorial, Eur. Phys. J. Spec. Top. **226**, 605 (2017).

[10] A. Bray and A. Rutenberg, Growth laws for phase ordering, Phys. Rev. E **49**, R27 (1994).
[11] A. J. Bray, Theory of phase-ordering kinetics, Adv. Phys. **51**, 481 (2002).
[12] D. Fisher and D. Huse, Nonequilibrium dynamics of spin glasses, Phys. Rev. B **38**, 373 (1988).
[13] C. Yeung, M. Rao, and R. Desai, Bounds on the decay of the autocorrelation in phase ordering dynamics, Phys. Rev. E **53**, 3073 (1996).
[14] S. Majumdar and D. Huse, Growth of long-range correlations after a quench in phase-ordering systems, Phys. Rev. E **52**, 270 (1995).
[15] G. Brown, P. Rikvold, M. Suton, and M. Grant, Evolution of speckle during spinodal decomposition, Phys. Rev. E **60**, 5151 (1999).